



# Failure analysis of high nickel alloy steel seal ring used in turbomachinery



Wenbo Wang<sup>a,b</sup>, Xiaolu Pang<sup>a,\*</sup>, Chengzhi Zheng<sup>a</sup>, Alex A. Volinsky<sup>a,b,\*\*</sup>

<sup>a</sup> Department of Materials Physics and Chemistry, University of Science and Technology Beijing, Beijing 100083, China

<sup>b</sup> Department of Mechanical Engineering, University of South Florida, Tampa, FL 33620, USA

## ARTICLE INFO

### Article history:

Received 10 November 2016

Received in revised form 24 February 2017

Accepted 10 March 2017

Available online 11 March 2017

### Keywords:

Seal ring

Failure

Precipitates

Recrystallization

High nickel alloy steel

## ABSTRACT

The purpose of this study is to identify the failure cause of the steel seal ring used in nuclear steam turbines. New high nickel steel alloy seal ring was compared with the failed seal ring. Metallographic analysis, scanning electron microscopy, nanoindentation and in-situ tensile testing were used to analyze the reasons of the seal ring failure at both macroscopic and microscopic scales. The main reason of the seal ring failure is a combination of stress and elevated temperature during turbine operation. Complex work environment caused recrystallization and recovery, resulting in grain refinement and secondary phases precipitation. Many secondary phase precipitates appeared at grain boundaries during use, causing formation of microvoids and cracks, ultimately leading to ring failure.

© 2017 Elsevier Ltd. All rights reserved.

## 1. Introduction

Seal ring is one of the important parts of power steam turbines, which is an elastic metal ring operating on the principle of outward expansion. Gas or liquid pressure is needed to form a good seal, as shown schematically in Fig. 1 [1]. The seal ring performance directly affects the safety and proper operation of the whole steam turbine unit. During operation, seal ring can be damaged due to long-term cyclic deformation, finally causing leakage. This article describes examples of the failure of the seal ring used in nuclear power turbines. The seal ring is made from the high nickel alloy steel, grade GH163 (YB/T 5351–2006 Chinese standard) [2]. The ring failure was manifested by high-frequency metal noise coming from the working nuclear power turbine. When the used free-standing seal ring was hit, similar crisp metal sound could be heard. Inspection revealed insufficient tension of the seal ring, associated with an incomplete seal. Designed opening gap length of the seal ring is 30–40 mm in the free state. Measured opening gap length of the used upper seal ring was 24 mm and the lower seal ring was 16 mm. As a result, the seal rings could not form a complete seal, causing leakage.

This study was commissioned to identify factors causing the seal ring failure. The seal ring failure was characterized using a series of experiments conducted at both macroscopic and microscopic scales. The same tests and characterization conducted with the new ring helped to analyze the failure mechanisms.

\* Corresponding author.

\*\* Correspondence to: A.A. Volinsky, Department of Materials Physics and Chemistry, University of Science and Technology Beijing, Beijing 100083, China.  
E-mail addresses: [pangxl@mater.ustb.edu.cn](mailto:pangxl@mater.ustb.edu.cn) (X. Pang), [volinsky@usf.edu](mailto:volinsky@usf.edu) (A.A. Volinsky).

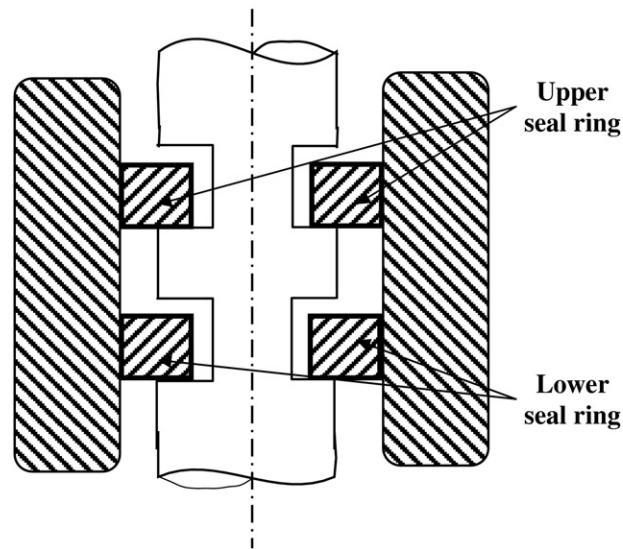


Fig. 1. Schematics of the seal rings in the nuclear power turbine system.

## 2. Methodology

Specimens were cut from the new and failed seal rings (Fig. 2), grinded with emery paper to 2000 grade and polished. In order to observe the microstructure, specimens were etched in mixed acid glycerin solution ( $\text{HCl}:\text{C}_3\text{H}_8\text{O}_3:\text{HNO}_3 = 3:3:1$  ratio) for 20 s [3].

Macroscopic ring dimensions were measured using calipers. Hardness and elastic modulus of the seal ring material were measured using nanoindentation. Specimens' microstructure, along with crack initiation and propagation were investigated by means of optical microscopy, scanning electron microscopy (SEM) equipped with energy-dispersive spectrometer (EDS) and in-situ SEM tensile testing (Camscan 3400).

## 3. Results and discussion

### 3.1. Macroscopic dimensions examination

Macroscopic and microscopic analyses were used to identify material failure. Table 1 lists measured diameter, width, opening gap length and gap lateral displacement of the failed and the new seal rings, shown in Fig. 3. While there are no obvious differences in the rings diameter, the opening gap length of the failed ring is larger, along with the gap lateral displacement. Thus, it is apparent that the used rings have undergone macroscopic plastic deformation, contributing to seal ring failure.

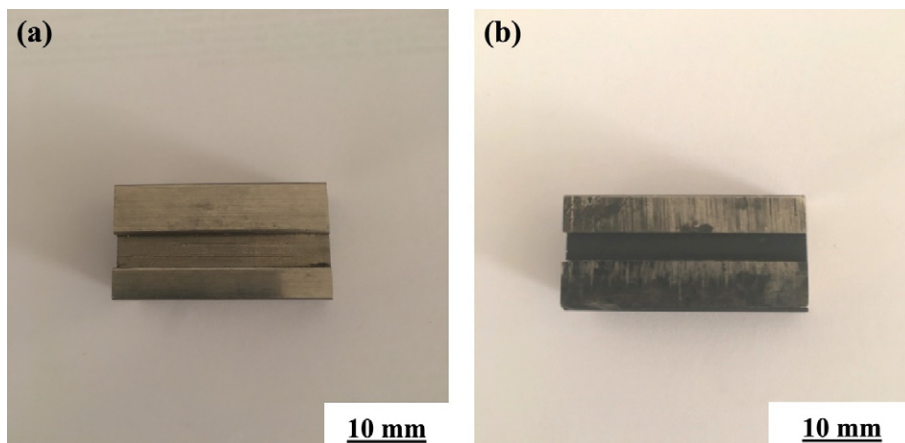
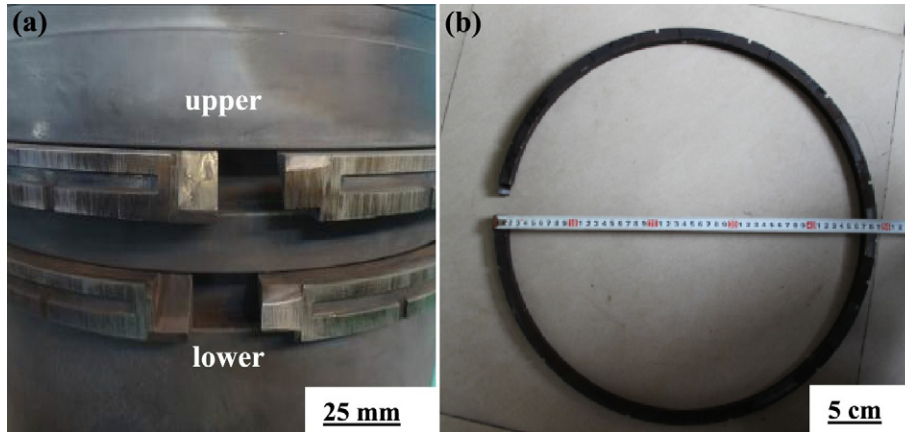


Fig. 2. Specimens cut from: (a) New seal ring; (b) Used seal ring.

**Table 1**  
Seal ring dimensions.

Parameter	Used 1	Used 2	New
External diameter, cm	48.9	49.3	49.52
Internal diameter, cm	46.1	46.39	46.25
Opening gap length, mm	25.94	31.86	29.68
Width, cm	1.89	1.88	2.11
Lateral displacement, mm	7.38	3.04	0



**Fig. 3.** (a) Upper and lower seal rings on the turbine; (b) Macroscopic ring dimensions measurements.

### 3.2. Relationship between the opening gap length and the applied load

The opening gap length of the seal ring was measured at different externally applied loads, shown schematically in Fig. 4, listed in Table 2. Based on the collected data, the relationships between the opening gap length and the applied load are shown in Fig. 5 for the used and new seal rings. It is clearly seen that the used rings are less stiff compared with the new ring. The stiffness change with use can be explained by the reduced ring width due to wear. The used rings were taken from

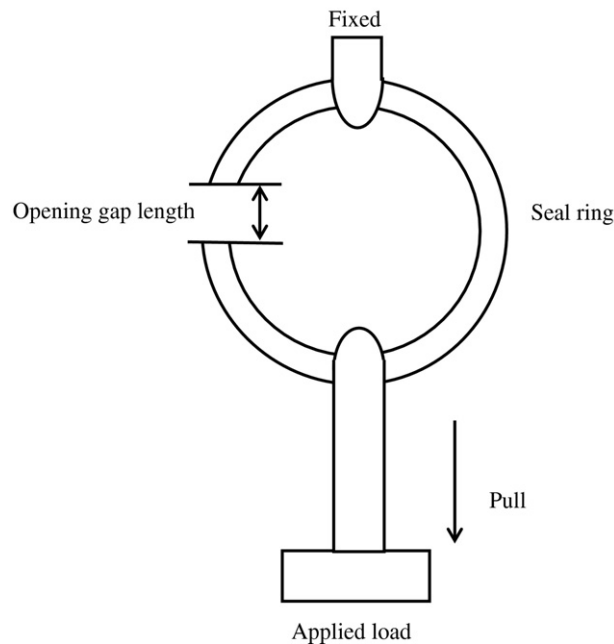


**Fig. 4.** Schematics of the opening gap length measurement method.

**Table 2**

Relationship between the externally applied load and the seal ring opening gap length.

Applied load, kg		0	0.6	1.6	2.6	3.6	5.6	7.6	10.6	15.6	20.6
Opening gap length, mm	U1	26.7	26.8	27.3	27.64	28.1	29.12	30.54	31.52	33.9	36.4
	U2	32.8	33	33.52	34.08	34.48	35.24	36.52	37.82	40.34	43.06
	N	30.12	30.2	30.42	30.78	30.98	31.28	31.9	32.66	33.78	35.08

Here, U1 means used ring 1; U2 is used ring 2, and N is the new unused ring.

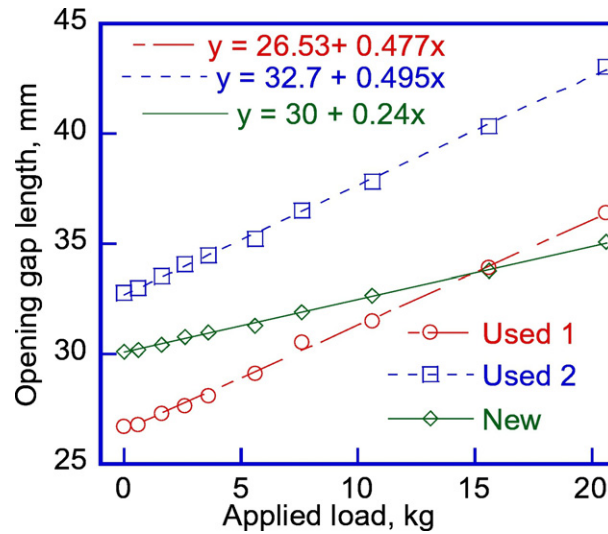


Fig. 5. Relationships between the opening gap length and the externally applied load.

the same failed turbine, which explains why both used rings have the same stiffness, and supports the argument that the change in the ring stiffness was due to wear.

### 3.3. Elastic modulus, hardness and bulk chemical composition

After grinding and polishing the specimens, the hardness and elastic modulus of the new and used seal ring materials were measured by nanoindentation. The results are presented in Tables 3 and 4. The elastic modulus and hardness of the new seal ring material are higher than the used one. The seal ring working environment is complex. The working pressure is 4.5–5.5 MPa and the temperature is 523–573 K. Hardness decrease with use can be explained by the recovery and recrystallization

**Table 3**

New seal ring mechanical properties.

Test	Elastic modulus, GPa ( $\pm 1$ )	Hardness, GPa ( $\pm 0.1$ )
1	306	4.9
2	305	5.2
3	323	5.1
4	329	5.1
Average	316	5.1

**Table 4**

Used seal ring mechanical properties.

Test	Elastic modulus, GPa ( $\pm 1$ )	Hardness, GPa ( $\pm 0.1$ )
1	265	3.3
2	303	3.3
3	267	3.1
4	271	3
Average	277	3.2

**Table 5**

Main elements composition of the used and new seal rings.

Elements		Fe	Cr	Ni	Mo	Cu	Ti
Composition, wt%	Used	54.5	15.27	24.64	1.52	0.69	2.85
	New	53.82	14.86	25.36	1.56	0.61	2.83

processes of the ring material at the microscopic scale. Bulk chemical composition of the new and used rings is listed in Table 5. There are no significant differences in chemical composition, so the reduction of the elastic modulus and hardness can be explained by the microstructure changes with use due to recovery, recrystallization and secondary phases precipitation. Used seal ring had been in service for 5 years under complex working environment. It is reasonable to assume that the used seal ring material was subjected to aging creep, i.e. over-aging, since long-term service and aging can cause significant hardness decrease [4].

During the nanoindentation test, the four points on the surface were randomly selected. The hardness of FCC nickel material at the nano-scale is significantly affected by crystallographic surfaces with different orientations. The hardness value of the (100) substrate is the greatest and the hardness values of the (111) substrate is the smallest. The reason is because the (100) substrate has only one slip angle of the {111} sliding planes and the (111) substrate has three slip angles, respectively, during nanoindentation, resulting in the (100) substrate having lower ability for plastic deformation, ultimately causing higher hardness value.

The used seal ring has been plastically deformed, resulting in stored strain energy. Also, there are many precipitates at grain boundaries. Both of these reasons can lead to lower hardness. Obtained experimental hardness values are within a reasonable range [5].

### 3.4. Metallographic, SEM and EDS analyses

Different surfaces of the seal ring were observed using optical microscopy and there were no obvious differences between the cross section, front and back surfaces, thus the back surface was used for microstructure comparisons. Fig. 6 shows optical images of the new and used rings back surface. Austenite grains can be clearly seen in both used and new rings, however, the new ring grain size in Fig. 6(a) is larger than the used ring in Fig. 6(b). The new seal ring average grain size is about 206  $\mu\text{m}$ , while the average grain size of the used seal ring is 62  $\mu\text{m}$ . The used seal ring has undergone serious grain refinement. Additionally, many precipitates can be observed at grain boundaries of the used ring in Fig. 6(b), opposite to the new ring in Fig. 6(a). Thus, it is reasonable to assume that the secondary phase precipitation occurred in the used rings along the grain boundaries, which is not present in the new ring. Compared with the new seal ring, the used seal ring material had many precipitates and more serious erosion of the grain boundaries due to the etching solution.

Regardless of the fact that the used steel ring grain size is significantly smaller than the new one, the used ring has lower hardness. It is reasonable to assume that the secondary phase precipitation occurred in the used rings, accompanied by high dislocation density due to use. While the operating temperature of 523–573 K is below steel recrystallization temperature [6], recovery affected the performance of the used seal ring. Because of the low operating temperature, atomic diffusion capacity is weak. However, the ring is also mechanically loaded during use, providing additional energy for dynamic recovery and recrystallization [7].

High nickel alloy steel material of the seal ring is austenitic steel with low stacking fault energy. Dynamic recovery is very slow because it is difficult for extended dislocations to escape from the dislocation network, and it is also difficult for dislocations to move by sliding and climbing. At the same time, high dislocation density in the sub-structure and the remaining energy can cause recrystallization. Thus, dynamic recovery and dynamic recrystallization soften the used seal ring material, as demonstrated by the hardness measurements [8,9].

SEM micrograph, elemental maps and EDS analysis of the used seal ring are presented in Fig. 7 to analyze the precipitates composition. Combined elements map is shown in Fig. 7(b), while individual elemental maps for Si, Fe, Cr, Ni, Ti and Mo are

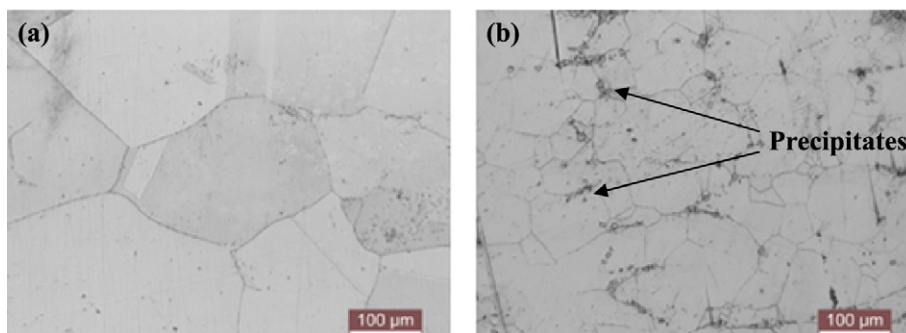
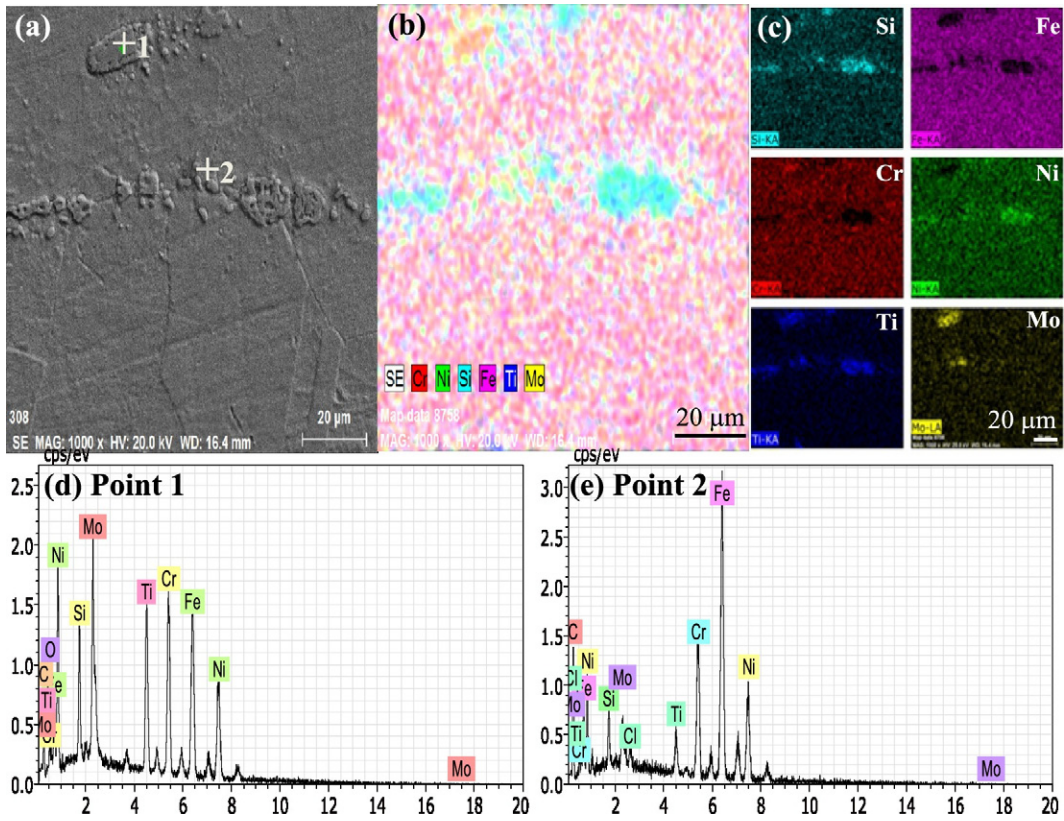


Fig. 6. Optical microscopy images of: (a) New seal ring back surface; (b) Used seal ring back surface showing precipitates along the grain boundaries.



**Fig. 7.** (a) SEM micrograph; (b) Combined elemental map; (c) Individual elemental maps; (d) EDS spectra of point 1 and (e) EDS spectra of point 2 of the used seal ring labeled in (a).

shown in Fig. 7(c). From the individual element maps it is clear that the precipitates composition is complex. EDS analysis results of points 1 and 2 in Fig. 7(a) are listed in Table 6, showing increased Ti and Mo concentrations. Moreover, the content of Ni, Si, Ti and Mo is higher in the precipitates regions along the grain boundaries, as seen in the combined and individual element maps in Fig. 7(b) and (c).

Unlike the used ring, no precipitation along the grain boundaries was observed in the new ring material. Table 7 lists elemental composition results of the new ring material obtained by EDS.

Compared with the used seal ring, there is much more Ni in the new seal ring steel. At the same time, Nb and Al can be found in the new seal ring material, which were not present in the used ring. Adding alloying elements, such as Al, Ti and Nb, to high nickel alloy steel, results in precipitation strengthening, producing secondary phase, while controlling over-saturated solid solution [10]. This is mainly based on the  $Ni_3Al$  intermetallic compound, called the  $\gamma$  phase. Al hardens high nickel alloy steel. However, the  $\gamma$  phase has higher solid solubility for Ti and Nb. Thus, adding them can reduce the effects of Al. Moreover, Nb can decrease the aging rate [11–15].

The seal ring maximum working temperature is around 573 K, which is not high enough to cause complete recrystallization. Thus, the mechanical stress of 4.5–5.5 MPa during operation needs to be considered. Combination of stress and temperature

**Table 6**

Used seal ring precipitate composition elements analysis by EDS.

Point 1	Conc. [wt%]	Conc. [at%]	Point 2	Conc. [wt%]	Conc. [at%]
C	11.74	36.32	C	23.92	59.1
O	3.01	6.98	Si	1.42	1.5
Si	3.02	4	Cl	0.46	0.39
Ti	11.24	8.72	Ti	2.67	1.65
Cr	15.54	11.1	Cr	11.1	6.34
Fe	22.86	15.21	Fe	38.43	20.42
Ni	20.58	13.03	Ni	19.38	9.8
Mo	12	4.65	Mo	2.61	0.81

**Table 7**

New seal ring composition elements analysis by EDS.

Point 1	Conc. [wt%]	Conc. [at%]	Point 2	Conc. [wt%]	Conc. [at%]
C	6.34	24.22	C	8.63	31.14
Al	0.83	1.42	Al	0.68	1.1
Ti	2.71	2.6	Cl	0.44	0.54
Cr	13.57	11.97	Ti	5.12	4.63
Fe	6.66	5.47	Cr	12.04	10.04
Ni	68.89	53.84	Fe	6.06	4.7
Nb	1	0.49	Ni	60.85	44.95
			Nb	6.17	2.88

causes the seal ring failure. As a final step to identify the cause of the ring failure, in-situ qualitative tensile test was conducted in SEM with new and used ring materials.

### 3.5. In-situ SEM tensile test

Identical tensile specimens, 22 mm long and 1 mm thick were cut from the used and new seal ring materials. In-situ tensile test and observation of the specimen surface proved that the grain boundaries are the weakest areas of the used seal ring material. During the tensile test, the specimens of seal ring transitioned from elastic to plastic deformation. Consistent with the nano-indentation hardness measurements, the yield stress of the used ring material was lower than the new ring material. Dislocations, fine-grain and precipitation could contribute to the lower used seal ring's yield strength. The precipitation can also contribute to the yield strength. The mechanism can be explained by the interaction between particles and dislocations [16]. Surface morphology of the used and new ring materials during the in-situ tensile tests is shown in Fig. 8.

Microvoids first appeared at the precipitates along the grain boundaries of the used ring material. Then microvoids aggregated, finally forming microcracks in Fig. 8(a). No such phenomena were observed in the new seal ring material in Fig. 8(b), where only grain boundaries can be seen without voids or cracks during the in-situ SEM tensile test. Therefore, precipitates are the main reason causing the seal ring failure and the grain boundaries are the weakest areas in the used seal ring. Microvoids aggregation eventually caused the formation of macroscopic cracks, leading to seal ring material failure.

## 4. Conclusions

Seal ring complex work environment, including temperature and stress, shows that the used seal ring lost its ability to form a complete seal, resulting in leakage and failure. Used seal ring obviously appears plastically deformed. Dynamic recrystallization of the used ring material caused grain refinement, which was reflected by reduced hardness. At the same time, precipitates appeared along the grain boundaries, leading to ring failure by forming cracks along the grain boundaries. The effects of precipitation contributed to grain refinement. Ti and Mo precipitates reduced the stacking fault energy, promoting dynamic recrystallization.

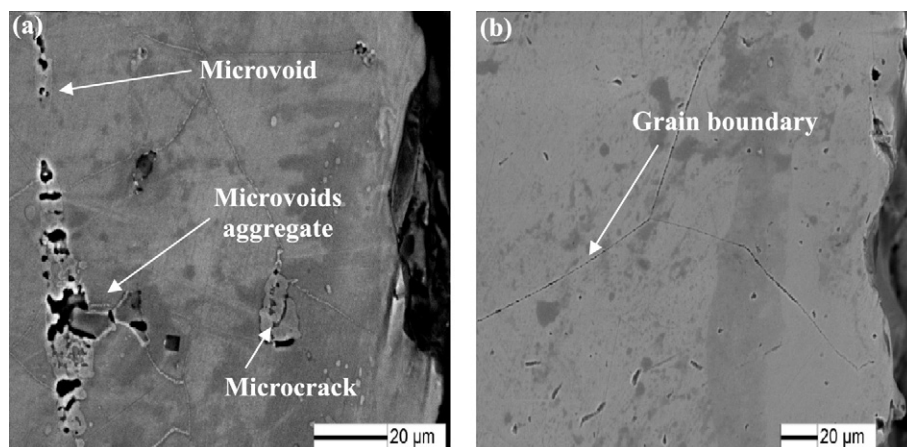


**Fig. 8.** SEM images of: (a) Used seal ring and (b) New seal ring obtained during in-situ tensile test.

## Acknowledgements

This research was supported by the National Natural Science Foundation of China (51271022, 51431004), Beijing Higher Education Young Elite Teacher Project (YETP0353), National Basic Research Program of China (2012CB937502) and by the National Science Foundation (IRES 1358088).

## References

- [1] N. Oishi, M. Tanaka, Periodic thermal deformation of large seal ring, *JSME Int. J. Ser. C, Dyn. Control, Robot. Des. Manuf.* 39 (2) (1996) 347–355.
- [2] Forged heat-resisting superalloy discs, YB/T 5351–2006 Chinese Standard, 2006.
- [3] M.B. Lin, K. Gao, C.J. Wang, A.A. Volinsky, Failure analysis of the oil transport spiral welded pipe, *Eng. Fail. Anal.* 25 (2012) 169–174.
- [4] Y.C. Lin, Y.C. Xia, Y.Q. Jiang, H.M. Zhou, L.T. Li, Precipitation hardening of 2024-T3 aluminum alloy during creep aging, *Mater. Sci. Eng. A* 565 (2013) 420–429.
- [5] C.H. Chen, The nanoindentation responses of nickel surfaces with different crystal orientations, *Mol. Simul.* 33 (11) (2007) 905–917.
- [6] Z. Larouk, H. Bouhalais, Recrystallization behavior of a low carbon steel wire, *Phys. Procedia* 2 (3) (2009) 1223–1229.
- [7] E. Cerri, P. Leo, Influence of severe plastic deformation on aging of Al–Mg–Si alloys, *Mater. Sci. Eng. A* 410 (2005) 226–229.
- [8] P. Zhang, C. Yi, G. Chen, H. Qin, C. Wang, Constitutive model based on dynamic recrystallization behavior during thermal deformation of a nickel-based superalloy, *Metals* 6 (7) (2016) 161, <http://dx.doi.org/10.3390/met6070161>.
- [9] C. Sun, Y. Xiang, Q. Zhou, D.J. Politis, Z. Sun, M. Wang, Dynamic recrystallization and hot workability of 316LN stainless steel, *Metals* 6 (7) (2016) 152, <http://dx.doi.org/10.3390/met6070152>.
- [10] B.H. Kear, D.P. Pope, Role of refractory elements in strengthening of  $\gamma'$  and  $\gamma''$  precipitation hardened nickel-base superalloys, *Superalloys Supercomposites Superceramics*, Academic Press 1989, pp. 545–582.
- [11] L. Luo, Y. Huang, S. Weng, F.Z. Xuan, Mechanism-related modelling of pit evaluation in the CrNiMoV steel in simulated environment of low pressure nuclear steam turbine, *Mater. Des.* 105 (2016) 240–250.
- [12] H. Bouaziz, O. Brinza, N. Haddar, M. Gasperini, M. Feki, In-situ SEM study of crack initiation, propagation and interfacial debonding of Ni–P coating during tensile tests: Heat treatment effect, *Mater. Charact.* 123 (2017) 106–114.
- [13] M.N. Ahmadabadi, H. Shirazi, H. Ghasemi-Nanesa, S.H. Nedjad, B. Poorganji, T. Furuhashi, Role of severe plastic deformation on the formation of nanograins and nano-sized precipitates in Fe–Ni–Mn steel, *Mater. Des.* 32 (6) (2011) 3526–3531.
- [14] B. Piekarski, Effect of Nb and Ti additions on microstructure, and identification of precipitates in stabilized Ni–Cr cast austenitic steels, *Mater. Charact.* 47 (3) (2001) 181–186.
- [15] S.L. Zhu, H.Z. Cao, J.S. Ye, W.H. Hu, G.Q. Zheng, Dynamic recrystallization behavior of medium carbon Cr–Ni–Mo–Nb steel during hot deformation, *J. Iron Steel Res. Int.* 22 (3) (2015) 264–271.
- [16] G. Sun, Q. Ma, In-situ observation of dark phase precipitation during heating and soaking process of a high nickel steel, *J. Wuhan Univ. Tech. Mater. Sci. Ed.* 30 (1) (2015) 152–155.